The 12th International Symposium on Transport Phenomena and Dynamics of Rotating Machinery
Honolulu, Hawaii, February 17–22, 2008

ISROMAC12–2008–20206

FLOW INSTABILITIES IN FEATHER SEALS DUE TO UPSTREAM HARMONIC PRESSURE FLUCTUATIONS

D. Deng[1], M.J. Braun[2], R.C. Hendricks[3]

[1]Design Engineer, reXorce Thermionics, Inc., Akron, OH 44311, Tel: 234–542–4554, ddeng@rexorce.com
[2]Professor of Mechanical Engineering, The University of Akron, Akron, OH 44325, Tel: 330–972–7734, mjbraun@uakron.edu
[3]Senior Technologist, NASA Glenn Research Center, Cleveland, OH 44135, Tel: 216–977–7507, robert.c.hendricks@grc.nasa.gov

ABSTRACT

Feather seals (also called slot seals) typically found in turbine stators limit leakage from the platform into the core cavities and from the shroud to the case. They are of various geometric shapes, yet all are contoured to fit the aerodynamic shape of the stator and placed as close as thermomechanically reasonable the powerstream flow passage. Oscillations engendered in the compressor or combustor alter the steady leakage characteristics of these sealing elements and in some instances generate flow instabilities downstream of the seal interface.

In this study, a generic feather seal geometry was studied numerically by imposing an upstream harmonic pressure disturbance on the simulated stator-blade gap. The flow and thermal characteristics were determined; it was found that for high pressure drops, large fluctuations in flows in the downstream blade-stator gap can occur. These leakages and pulsations in themselves are not all that significant, yet if coupled with cavity parameters, they could set up resonance events. Computationally generated time-dependent flow fields are captured in sequence video streaming.

INTRODUCTION

Brush, finger, and leaf seals are representative of conventional compliant seals. They have potential hydrodynamic lifting capabilities, a non-contacting nature, and theoretically unlimited lifespan. Their configurations, modeling, and applications are described in a large body of literature: for example, Braun et al. (2005), Hendricks et al. (2006), and Nakane et al. (2004), while a good review of nozzle guide vane seal configurations is given by Farahani and Childs (2006). Feather seals, however, have a configuration similar to that of placing a thin metal sheet between each slot cut in each segment of adjacent stators, Tibbott and Gates (1996). It is desirable to cool the surrounding segment and the feather seal itself with minimum leakage and negative effect on the gas turbine. This paper studies via the Colburn factor the flow and implicit thermal behavior of a typical feather seal by superimposing an upstream harmonic pressure disturbance over a steady pressure amplitude.

GEOMETRY

The geometry of the feather seal is presented in Figure 1. The clearance coefficient A varies from 0.3 to 0.5 and 0.7, respectively, which means the clearance can be 0.024, 0.04 and 0.056 mm, respectively. The length of the narrow path is 2.6 mm. The geometry is symmetric about the horizontal center line. In reality the clearance varies with engine operations, yet for this analysis the clearance is fixed.

NUMERICAL IMPLEMENTATION

The numerical algorithm used in the present calculations, CFD-ACE+, is a commercial software package, which solves the full incompressible or compressible Navier-Stokes equations in a body-fitted Cartesian coordinate system. The finite-volume approach employs an algebraic multi-grid solver that allows as many as 50 internal sub-iterations for both the velocity and pressure correction equations. The adoption of the finite-volume approach is especially attractive because of the fact that it allows a conservative formulation for the discretized governing Navier-Stokes equations. First-order upwind scheme is adopted for the discretization of the convective terms because of its nature of stability. This solution procedure applies to both incompressible and compressible flows. The 2D X-Y grid was adopted for the computational domain. Grid-convergence experiments were performed to ensure that the results are grid independent. Eventually 7X140 and 200X100 nodes are chosen for the small clearance and the large clearance passages, respectively. The total grid contains 534 nodes in the X-direction and 420 nodes in the Y-direction. The number of total quad cells is 71,882 for the whole domain. No turbulence model [Direct Numerical Simulation (DNS) scheme] was adopted for both incompressible and compressible flows.

BOUNDARY CONDITIONS

The left-hand side of Figure 1 represents the high-pressure side, which is set as an inlet boundary condition with oscillating pressure $P_{in} = P_0\left[1 + a\sin(2\pi ft)\right]$. Here a is amplitude and f frequency of the oscillation, with P_0 the upstream stagnation pressure. The right-hand side represents the low-pressure side, which is set as an outlet boundary condition with pressure $P_{out} = 0$. All the other sides of the geometry are set as non-slip wall boundary conditions.

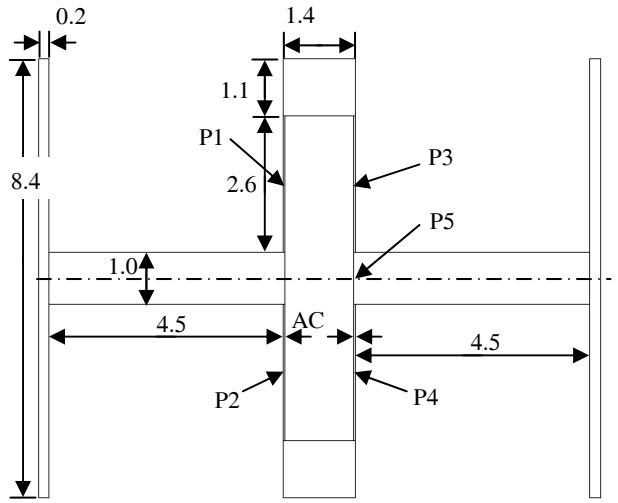

Figure 1.—Geometric description of the feather seal. (1) Units are in millimeters. (2) C = 0.08 mm. (3) A = 0.3, 0.5, or 0.7.

RESULTS AND DISCUSSION

Figure 2 presents, for an incompressible flow, the contours of velocity magnitude at different dimensionless times ($t^* = t/T$, $T = 1/f = 0.01$ s) for the case of A = 0.5, $P_0 = 5\times10^4$ N/m^2, $a = 0.05$, $f = 100$ Hz. It shows the process of the backward pulsation flow. At the beginning, the flow on the low-pressure side is symmetric before it reaches the outlet, and the flow on the high-pressure side is not symmetric because the velocity in the clearances [high length to clearance (L/C) passages] is not large enough to pass the flow (the flow is "blocked" by the clearances), Figure 2(a). The flow on the low pressure side begins to pulsate after it reaches the outlet, and the non-symmetry of the flow on the high pressure side decreases with an increase of the velocity in the clearances, Figure 2(b). The pulsation of the low pressure side flow "transports" upstream with the further increase of time, while the high pressure side flow becomes symmetric, Figure 2(c). The flow pattern is fully developed when t^* = 0.12, and only the magnitude of the velocity oscillates with the oscillation of the upstream pressure, Figure 2(d).

Figure 3 presents the contours of the stream function corresponding to the velocity magnitude shown in Figure 2. It shows the same process of backward pulsation flow; that is, the flow in the low pressure side is symmetric before it reaches the outlet, it pulsates when it reaches the outlet, and then the pulsation "transports" upstream until it is fully developed.

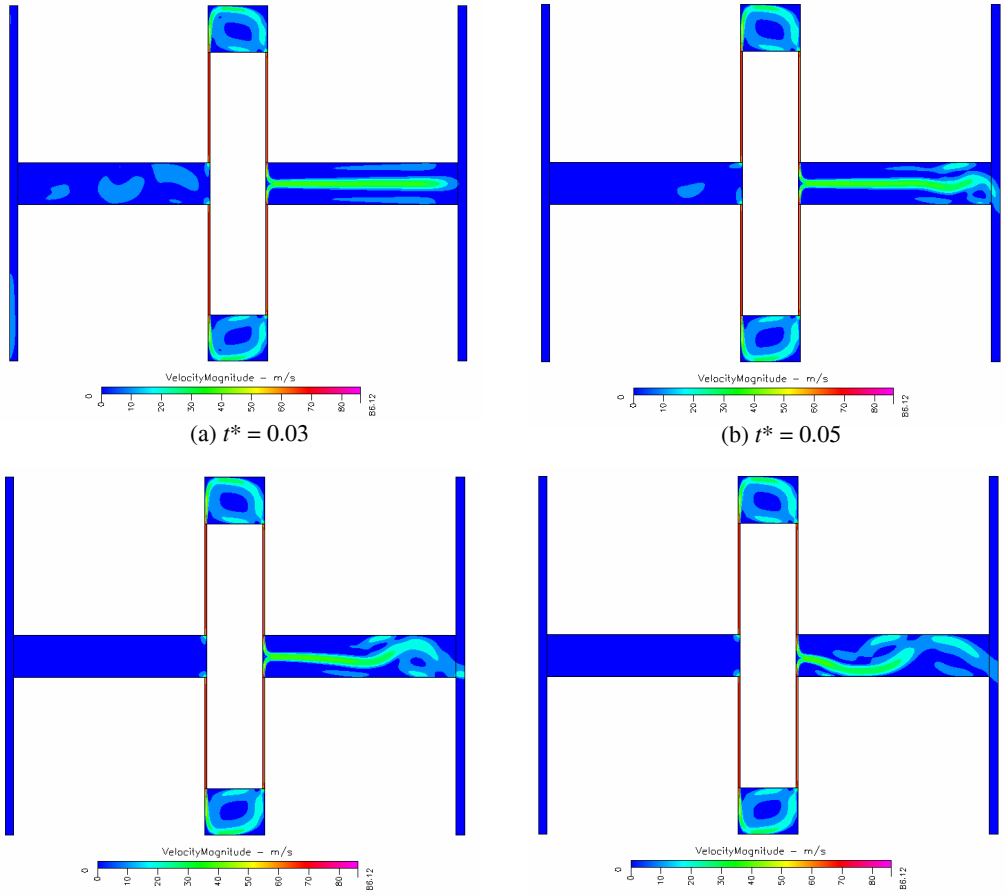

(a) t^* = 0.03 (b) t^* = 0.05

(c) t^* = 0.08 (d) t^* = 0.12

Figure 2.—The contours of velocity magnitude at different time ($P_0 = 5\times10^4$ N/m^2, $a = 0.05$, $f = 100$ Hz and incompressible flow).

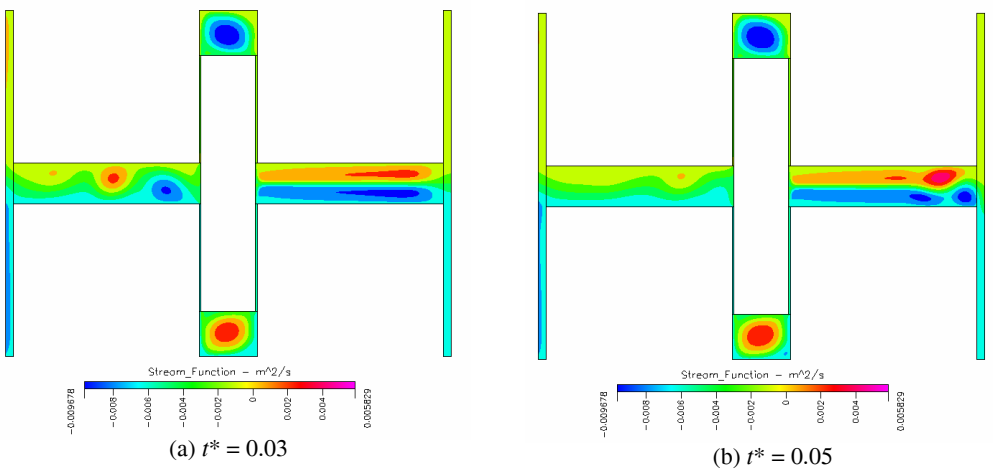

(a) $t^* = 0.03$ (b) $t^* = 0.05$

(c) $t^* = 0.08$ (d) $t^* = 0.12$

Figure 3.—The contours of stream function at different time ($P_0 = 5\times10^4$ N/m^2, $a = 0.05$, $f = 100$ Hz and incompressible flow).

Figures 4 and 5 present, for compressible flow, the contours of velocity magnitude and stream function vs. time for the case of A = 0.5, $P_0 = 5\times10^4$ N/m^2, $a = 0.05$, $f =$ 100 Hz. The flow pattern is similar to that of the incompressible case shown in Figures 2 and 3. The difference is that the flow on the low-pressure side begins to be non-symmetric when $t^* = 0.05$, which happens before it reaches the outlet, Figures 4(b) and 5(b). Also, the largest velocity magnitude and stream function for the compressible flow are larger than those of the incompressible flow: 130.3 m/s vs. 86.12 m/s and 0.008277 m^2/s vs. 0.005829 m^2/s, respectively.

Figure 6 presents, for both of the compressible and incompressible cases, the pressure-time history for one and one-quarter period at five different locations P_i, shown in Figure 1. It is shown that the pressure of the compressible case is always larger than that of the incompressible case at all five points. Also, the amplitude of the pressure oscillation for the compressible flow is always larger than that of the incompressible case: for example, 1,900 N/m^2 vs. 1,350 N/m^2 at P1 for compressible and incompressible cases, respectively. It is also shown that there is a transition stage when the pressure is increasing significantly for the case of compressible flow. This stage coincides with the formation of the flow pattern ($t^* < 0.12$) shown in Figures 4 and 5. There is no such transition stage for the case of the incompressible flow. Also note that the pressure oscillates drastically during the formation of the flow pattern ($t^* < 0.12$) at P5 for both compressible and incompressible cases, Figure 6(c). Finally, there is surprisingly little change in phase between the two cases.

Figure 7 presents the pressure-time history for one period at five different locations for the cases of (i) $P_0 = 5\times10^4$ N/m^2, $a = 0.05$ and (ii) $P_0 = 5\times10^5$ N/m^2, $a = 0.1$, respectively. Both cases are for incompressible flow. It is shown that the pressure profiles are not much different at P1 and P2 for the two cases, Figures 7(a) and 7(b). The pressure at P3 and P4 for case (ii) oscillates at the same primary frequency with subharmonic frequencies, Figure 7(d), while for case (i) there are no subharmonic frequencies, Figure 7(c). However, the pressure oscillates during the formation of the flow pattern ($t^* < 0.12$) at both P3 and P4 for case (i), Figure 7(c). The pressure at P5 for case ii) is random, and the primary frequency is not

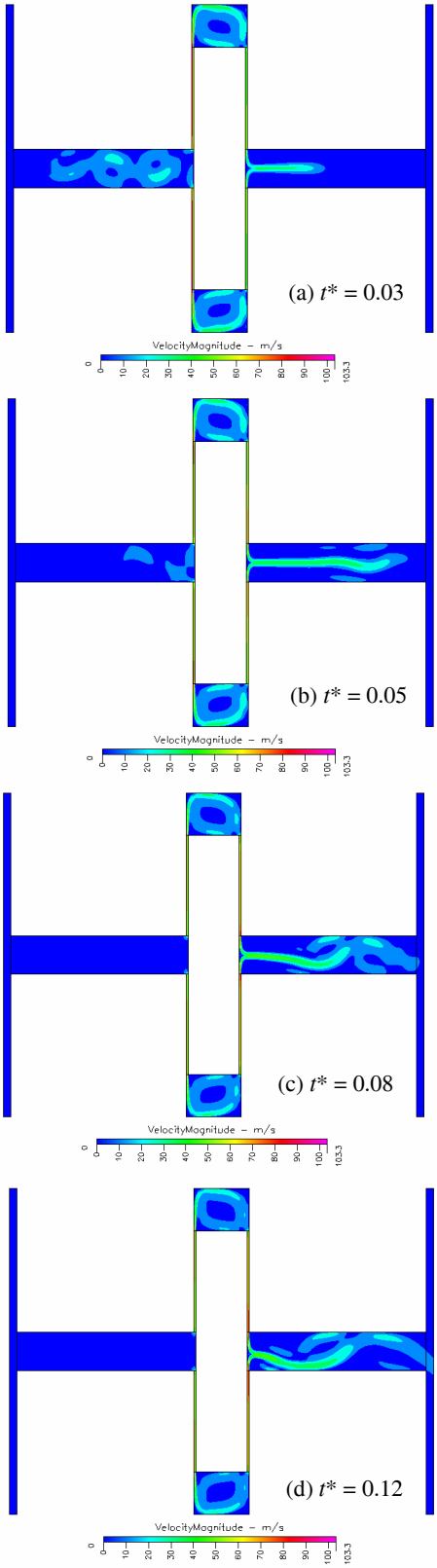

Figure 4.—The contours of velocity magnitude at different time ($P_0 = 5\times10^4$ N/m^2, $a = 0.05$, $f = 100$ Hz and compressible flow).

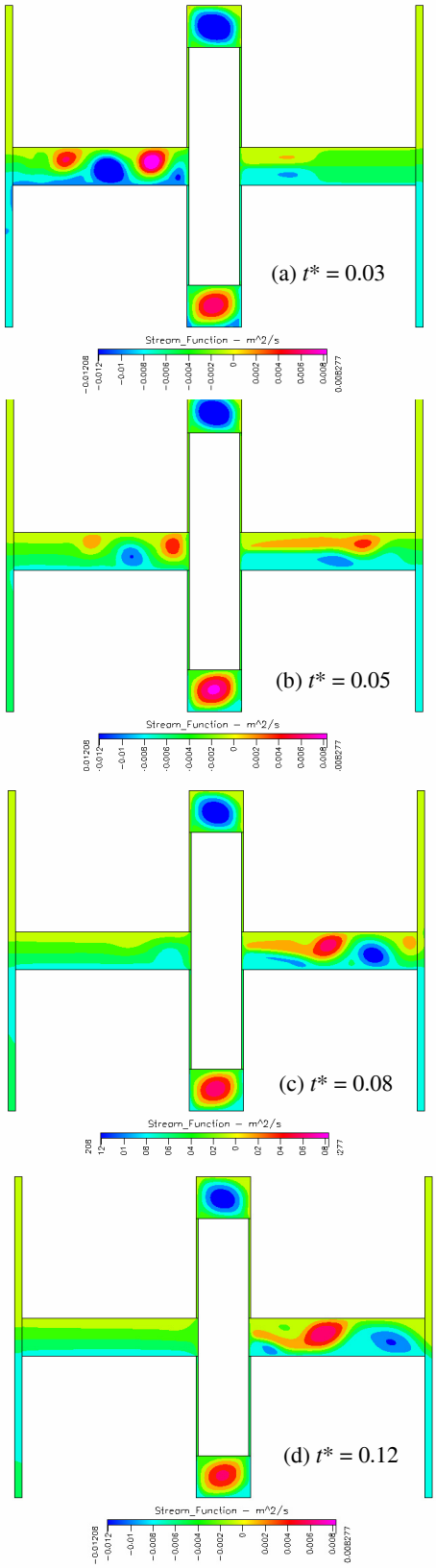

Figure 5.—The contours of stream function at different time ($P_0 = 5\times10^4$ N/m^2, $a = 0.05$, $f = 100$ Hz and compressible flow).

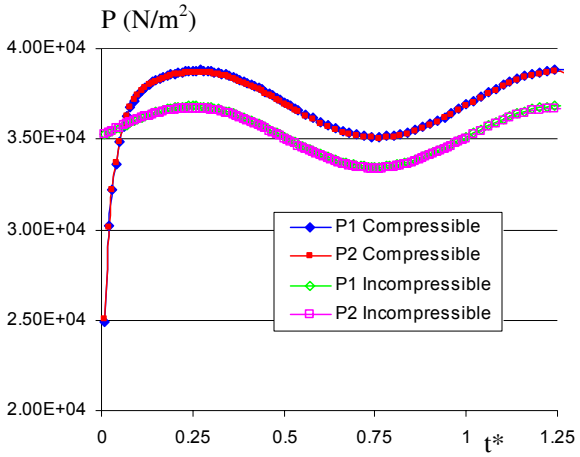

(a) P1 and P2

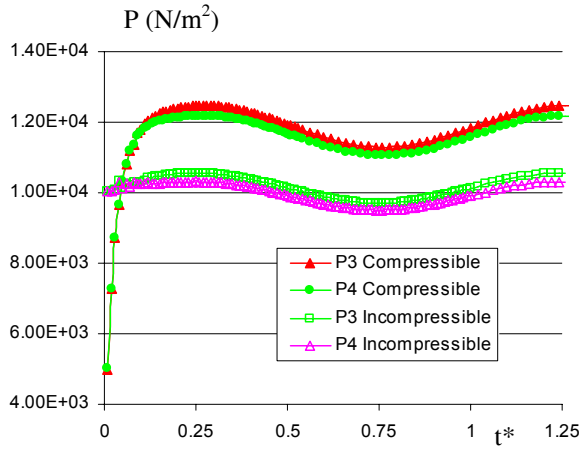

(b) P3 and P4

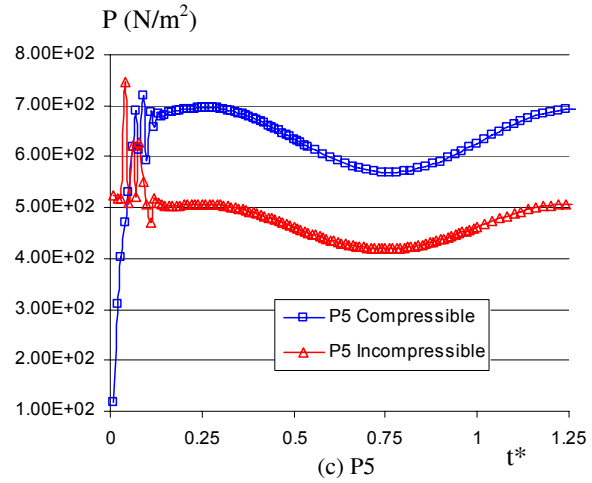

(c) P5

Figure 6.—Pressure vs. time at different locations ($P_0 = 5\times10^4$ N/m^2, $a = 0.05$, $f = 100$ Hz).

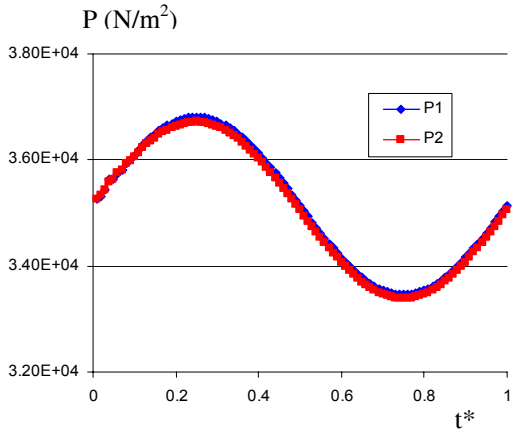

(a) $P_0 = 5\times10^4$ N/m^2, $a = 0.05$

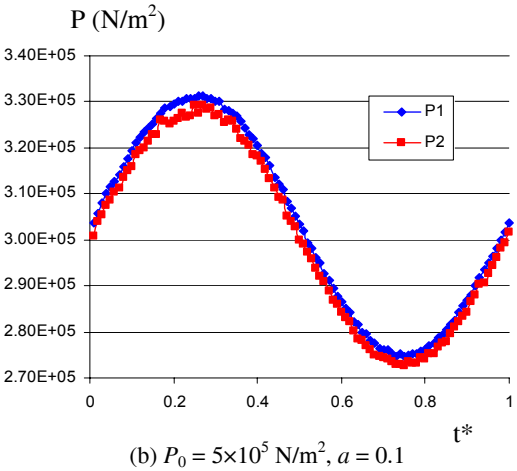

(b) $P_0 = 5\times10^5$ N/m^2, $a = 0.1$

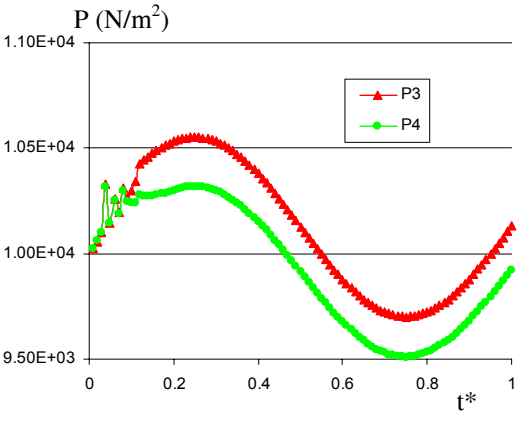

(c) $P_0 = 5\times10^4$ N/m^2, $a = 0.05$

Figure 7.—Pressure vs. time at different locations (incompressible flow).

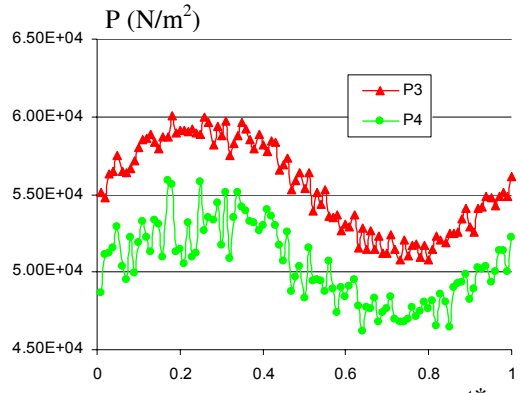

(d) $P_0 = 5\times10^5$ N/m^2, $a = 0.1$

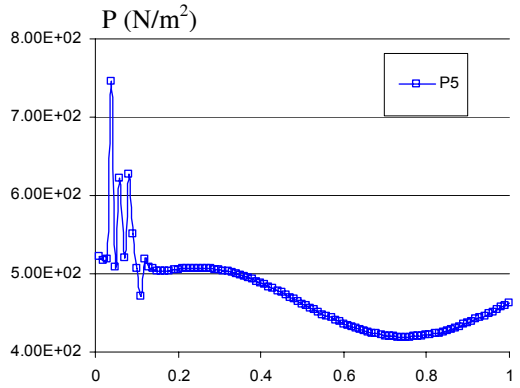

(e) $P_0 = 5\times10^4$ N/m^2, $a = 0.05$

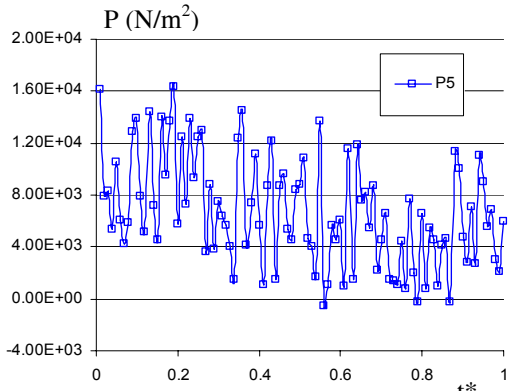

(f) $P_0 = 5\times10^5$ N/m^2, $a = 0.1$

Figure 7.—Continued. Pressure vs. time at different locations (incompressible flow).

discernible because of the turbulent nature of the flow, Figure 7(f). However, the pressure at P5 for case (i) still oscillates at the same frequency with that of the inlet pressure, except that the pressure changes drastically during the formation of the flow pattern, Figure 7(e).

Figure 8 presents the mass flow rate vs. time for both the incompressible and compressible cases. It is shown that the mass flow rate for the compressible case is much larger than that of the incompressible case, 6.62×10^{-3} vs.

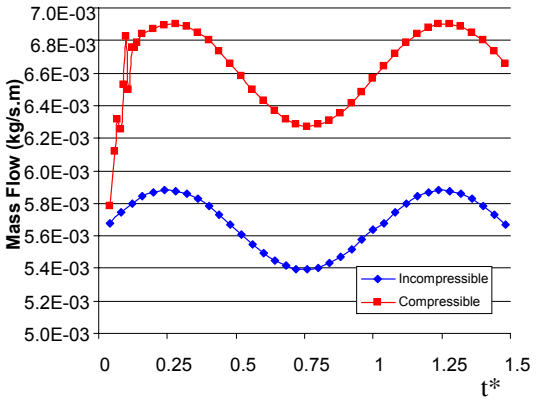

Figure 8.—Mass flow vs. time for incompressible and compressible flow ($P_0 = 5\times10^4$ N/m2, $a = 0.05$, $f = 100$ Hz).

5.64×10^{-4} kg/(s·m). Also, the mass flow rate increases rapidly during the formation of the flow pattern for the case of the compressible flow.

When combining the effects of the pressure perturbations of Figure 7(f) and the jetting effects of Figures 2 and 4, it is apparent that the flows are unsteady and can lead to unstable flows within the cavity regions. These oscillating flows, if compounded with corrosive gases or micro- or nano-particulates can promote an erosive action at the sealing interface that can also pump foreign matter into the outlet cavities. Unstable flows also engender noise, which can couple with other oscillations with a potential to resonate. Both the erosive effect and the potential to resonate limit the life of a system and need to be considered early in the design phase.

The mass flow rate (or leakage) acts as a coolant for the seal and the sub-platform region. The dynamics at P1–P4 are not all that different between compressible and incompressible flows, and the mass flows closely follow the square root law of the pressure ratio at the exit P5 shown in Figure 6(c). Some instabilities are noted in the initial phase of the compressible solution.

Through the Colburn analogy, the heat transfer would be higher for compressible flow and in either case follows in phase with the sinusoidal amplitude of the pressure pulse. The oscillatory behavior would engender component fatigue and enhanced corrosive gas attack on the material interfaces.

CONCLUSIONS

The flows within a feather or slot seal with a perturbed upstream pressure have been investigated. While the upstream responses on the average are uniform, the local values are time dependent with unstable jetting on the downstream side of the slot passage interface.

Local pressure dynamics are similar for both compressible and incompressible flows, except at the seal outlet where the mass flows closely follow the square root law of the pressure ratio; here they are higher for compressible flow.

The oscillatory behavior of particulates or corrosive gases within the narrow sealing gaps enhance the local heat transfer coefficients engendering wear that degrades component life. As such, perturbed behavior needs to be considered early in the design phase of the component sealing interface.

ACKNOWLEDGEMENT

The authors are grateful to Dr. Dzu K Le, NASA Glenn Research Center for assistance in investigating the pressure-time dependence, Dr. Meng-Sing Liou for assistance in CFD coding and discussions with Dr. Florin Dimofte.

REFERENCES

Braun, M.J., Pierson, H.M. and Deng, D. (2005), Thermofluids Considerations and the Dynamic Behavior of a Finger Seal Assembly, *Tribology Transactions*, vol. 48, pp. 531–547.

Farahani, A. and Childs, P. (2006), Nozzle Guide Vane Static Strip Seals, GT2006–90185, ASME Turbo Expo 2006, Barcelona, Spain.

Hendricks, R.C., Braun, M.J., Deng, D. and Hendricks, J.A. (2006), Compliant Turbomachine Sealing, ISROMAC–11, Honolulu, HI.

Nakane, H., Maekawa, A., Akita, E., Akagi, K., Nakano, T., Nishimoto, S., Hashimoto, S., Shinohara, T. and Uehara, H. (2004), The Development of High-Performance Leaf Seals, Transaction of ASME, Journal of Engineering and Gas Turbines and Power, vol. 126, pp. 342–350.

Tibbott, I. and Gates, R. (1996), Gas Turbine Engine Feather Seal Arrangement, United States Patent No. 5,531,457, July 2, 1996.